
FINE TUNING THE PHYSICAL PROPERTIES (STRUCTURAL AND MAGNETIC) OF SOL-GEL DERIVED COBALT FERRITE (COFe₂O₄) USING CALCINATION.

Khushboo Kumari

S.V.P College Bhabhua, Veer kunwar Singh University, Ara, Bihar, India

Kumar Raj Chittaranjan Singh

Narayan Mahavidyalaya, Siwan, Jai Prakash University, Chhapra, Bihar, India

Pankaj Varshney

SRM Institute of Science and Technology, Delhi-NCR Campus, Modinagar, U.P, India.

Manorma Chauhan

Govt. Girls P.G.College Rampur, U.P ,India

Raj Kumar Gupta*

*S.V.P College Bhabhua, Veer kunwar Singh University, Bihar, India

Sudhir Kumar

S.V.P College Bhabhua, Veer kunwar Singh University, Bihar, India

Harendra Satyapal*

*S.V.P College Bhabhua, Veer kunwar Singh University, Bihar, India

***Corresponding author:** Raj Kumar Gupta, Harendra Satyapal

Email: rajkgsw66@gmail.com, satyapal3976@gmail.com,

Abstract

Spinel Cobalt ferrite (CoFe₂O₄) is made via a sol-gel technique based on citrate precursors and further calcined at 600, 700, and 800°C for two hours. Purity of materials with spinel crystal symmetry indexed to *Fd3m* space group is confirmed by the X-ray diffraction pattern. To determine the size of crystallites and the lattice strains present in samples, the Williamson-Hall plot is analysed. The lattice parameters exhibits observable increase as a result of induced lattice strain, with sample calcined at 800°C having maximum value. WH analysis is backed by SEM morphological images. The FTIR spectrum and the XRD data are also in agreement. Samples' magnetic properties range from magnetization values of 47.62 to 71.11 emu/g and retentivity values of 21.19 to 37.16 emu/g. The increased value of coercivity from 454 to 1467 Gauss due to controlled calcination is interesting. Consequently, the impact of calcination temperature on CoFe₂O₄ for improvement of its physical properties is explored in this paper.

Keywords: Spinel ferrite, Coercivity, Sol-gel, Ferrimagnetic, Magnetization

1. Introduction

Applications for ferrimagnetic spinel ferrites include magnetic recorders, MRI scans, biosensors, magneto-optical devices, and more [1–5]. Due to its strong saturation magnetization and coercivity, cobalt ferrite is the spinel ferrite family's most studied magnetic substance [6]. With a paramagnetic to ferrimagnetic transition temperature of ~ 798 K, cobalt ferrite (CoFe_2O_4) exhibits ferrimagnetic properties [7]. With the space group $Fd3m$, cobalt ferrite crystallizes in a mixed spinel form. The typical formula for spinel cobalt ferrite is AB_2O_4 , where A stands for a tetrahedral site and B for an octahedral site, both of which are surrounded by 4 and 6 oxygen ions, respectively. CoFe_2O_4 has 64 tetrahedral sites and 32 octahedral sites in a single crystal, of which 8 tetra and 16 octahedral sites are occupied by metal cations and the remaining sites by oxygen ions [8]. Numerous studies have focused on replacing the Co^{2+} and Fe^{3+} sites with any metal cations in order to modify the magnetic characteristics of CoFe_2O_4 based on the distribution of cationic species between the tetrahedral and octahedral sites. Cobalt or iron ion substitution can be used to fine-tune the physical characteristics of CoFe_2O_4 . Co^{2+} ions prefer octahedral positions, however their presence on the B site of the spinel ferrite results in significant magnetoanisotropy energy in the CoFe_2O_4 lattice [9].

I.C.Nlebedim et al. discovered in 2010 that the redistribution of cations in the CoFe_2O_4 crystal lattice led to an increase in magnetization and a decrease in anisotropy [10]. It's vital to note that synthesis methods have also been implicated in altering CoFe_2O_4 's physical properties [11]. According to literature surveys, cations are substituted with transition elements in research projects aimed at changing the physical characteristics of cobalt ferrites [12–16]. To the best of our knowledge, there is little published material that discusses calcination in the crystal lattice as a means of improving the physical features of cobalt ferrite. So, in this article, we describe the sol gel auto combustion method we used to create pure phase spinel cobalt ferrite. Finding a correlation between the influence of calcination and improvements in the physical characteristics of cobalt ferrite has been our primary emphasis.

2. Experimental details

2.1. Materials and method

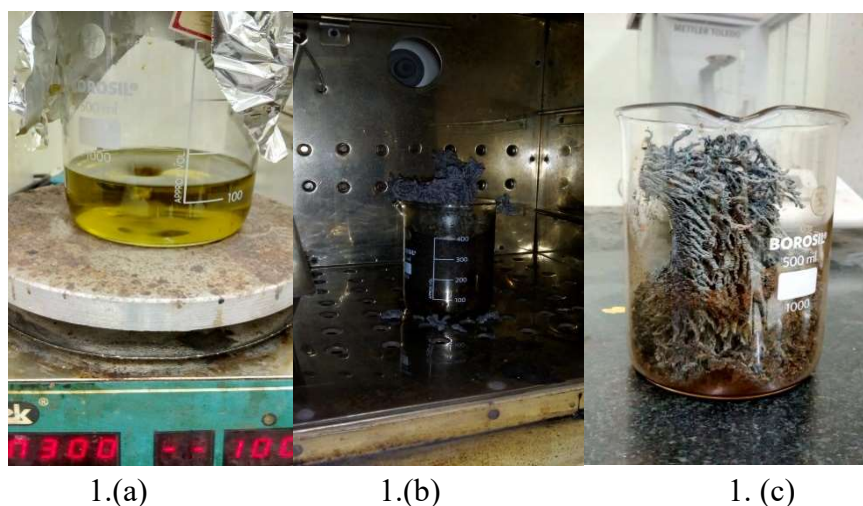


Fig.1. Synthesis (a) reactants on magnetic stirrer (b) gel combustion in hot air oven (c) ferrite tree

Using a low-cost chemical-based auto combustion sol-gel technique, the pure phase CoFe_2O_4 was created. $\text{Co}(\text{NO}_3)_2$ and $\text{Fe}(\text{NO}_3)_3$ (99.9% purity) were the high purity chemicals employed in this synthesis procedure. Citric acid and cations were assumed to have a molar ratio of 1:3. A calculated ratio of chemicals was weighed and added to small beakers of deionized water in each beaker. These aqueous iron, cobalt, and cerium nitrate solutions were then added to the beaker containing the citric acid solution. The pH of this final solution is then changed to 7 by adding ammonia drop by drop (Fig 1.a-c). Finally, a thick jelly-like product was produced by keeping this prepared solution on a hot plate stirrer under constant stirring at a temperature of $120\text{ }^\circ\text{C}$ for (4-5) hours. After being held in a hot air oven chamber at $250\text{ }^\circ\text{C}$ for two hours, the viscous jelly-like product expanded into a frothy substance under the control of a self-propagating combustion reaction. The result is a thick, ash-like powder (Fig 1.c) that is then further ground with a mortar and pestle into fine granules. The powdered samples were then placed in separate alumina crucibles and heated to 600 , 700 , and $800\text{ }^\circ\text{C}$ for two hours each in a microprocessor-based annealing furnace with a heating rate of $4^\circ\text{C}/\text{min}$. Finally, these prepared nanomaterials were given for material characterizations.

2.2. Characterizations

The room temperature X-ray diffraction patterns were obtained at a wavelength ($\lambda=1.5406\text{ \AA}$) using the Bruker X-ray Diffractometer. Magnetic hysteresis loops were carried out using Vibrating Sample Magnetometer capable of the magnetic field up to 2 Tesla. The surface morphology of the nanomaterials was examined with SEM (Carl Zeiss). The functional groups analysis done using Fourier Transform Infrared Spectroscopy (FTIR, Perkin Elmer).

3. Results and discussion

3.1. X-ray diffraction analysis

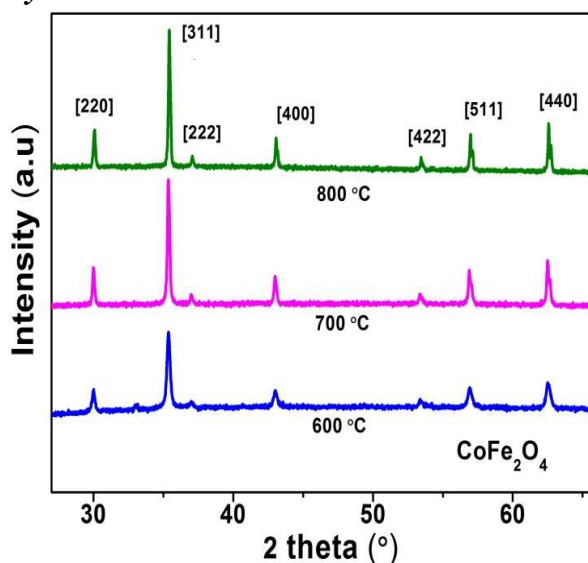


Fig. 2. XRD pattern of CoFe_2O_4 at three different temperatures.

As illustrated in Fig. 2, X-ray diffraction peaks demonstrate that all produced nanomaterials are in pure phase, have spinel crystal structures, and fall under the space group $Fd3m$. Peaks of X-ray intensity are consistent with earlier reports [17]. As the calcination temperature rises, the XRD intensity peak broadening decreases monotonically. The signature planes (220) and (311) are increased by the temperature effect, as is clear from Fig. 1. The most intense planes (311) can also be seen shifting to a lower Bragg's angle. This might be the result of lattice strain that the samples' high-temperature heating caused to grow. The magnetic characteristics are hypothesised to be affected by the change in lattice parameters because it alters the distance between magnetic ions, which alters the super exchange interactions between Fe^{3+} ions.

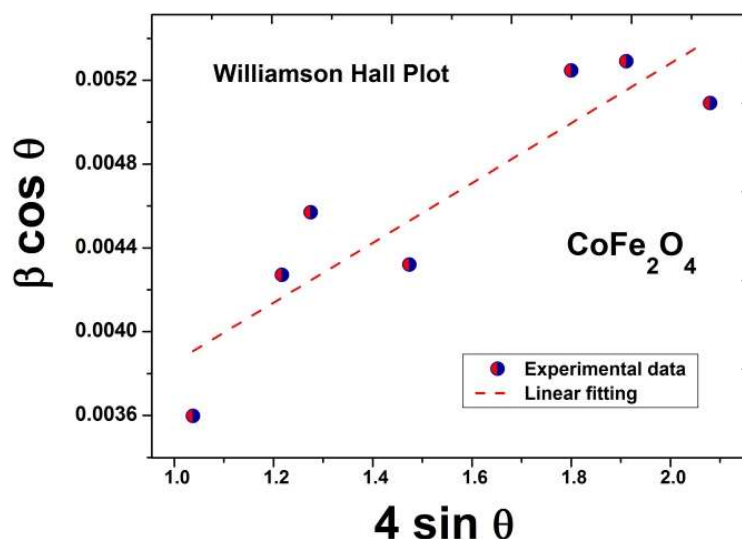


Fig. 3. WH plot of CoFe_2O_4 for sample calcined at 800°C

The crystallites size and lattice strains in samples were determined using Williamson-Hall plotting (Fig.3). The Williamson-Hall equation is expressed as [17].

$$\beta \cos \theta = K \lambda / D + 4 \varepsilon \sin \theta \quad (1)$$

Where, λ is the wavelength of X ray, θ is the Bragg's angle. D denotes crystallite size and β is (FWHM) of intensity versus 2θ plot. The term $(4\varepsilon \sin \theta)$ is strain effect and value of intercept on the ordinate axis is equated with $(K\lambda/D)$ to find the crystallite sizes.

The calculation of lattice constants for this particular spinel crystal system is done using equation (2). The lattice parameter (a), and subsequently the lattice volume, may be seen to have noticeable increases but is of comparable magnitude for sample $700\text{-}800^\circ\text{C}$. These findings are consistent with bond stretching revealed through FTIR analysis. With calcination temperature, crystallite size rises. This might be a result of the agglomerations brought about by thermal activations, as shown by the SEM morphological analysis (detailed later). The average crystallite size for these samples are 56.46 nm. The summarized structural details are tabulated in Table 1.

$$\frac{1}{d^2} = \frac{4}{3} \left(\frac{h^2 + hk + k^2}{a^2} \right) + \frac{l^2}{c^2} (2)$$

The planes used in his equations were [311], [220], [511], [440] and [422]. The analysis of X-ray intensity patterns of samples were performed keeping the *Fd3m* space group as the reference.

Table 1. Structural details of CoFe_2O_4

Calcination (°C)	Crystallite size (WH plot)nm	Strain $\times 10^{-3}$	Crystal structure details	
			$a=b=c(\text{Å})$	cell volume(Å^3)
600	48.1 (± 1)	1.08	8.373	587.006
700	57.96 (± 1)	2.62	8.367	585.745
800	63.32 (± 1)	2.05	8.369	586.166

3.2 SEM analysis

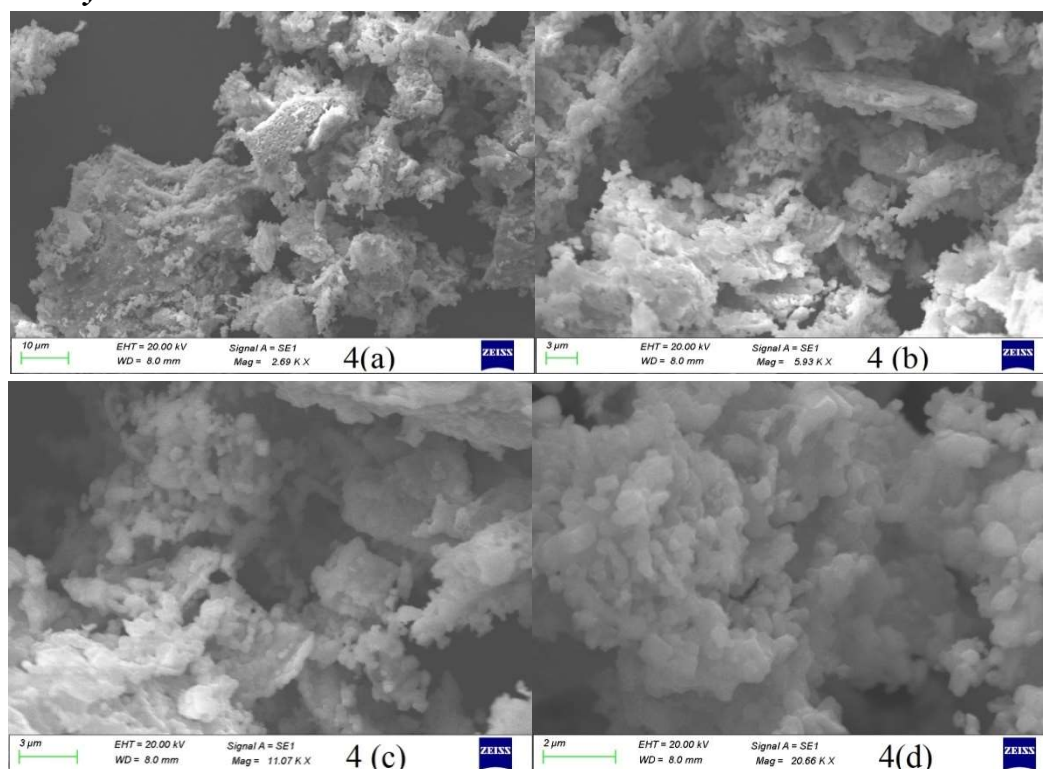


Fig. 4(a-d). SEM micrograph of CoFe_2O_4 calcined at 800°C

The particle size and the crystallite size, as measured by the W-H plot, are typically not the same. The crystallite size obtained using W-H plots is thus supported by SEM micrographs. As a result, Fig. 4(a-d) shows a sample of CoFe_2O_4 in an electron microscope at various magnifications. Samples appear to aggregate as a result of annealing because nanocrystals attempt to lower their energy state by reducing their interfaces with neighboring particles [25]. The SEM data show

larger particle sizes as compared to the XRD values. The average particle size of CoFe_2O_4 is 88.06 nm. Using imageJ software and visualizing concern histograms, particle size is calculated.

3.3 FTIR analysis

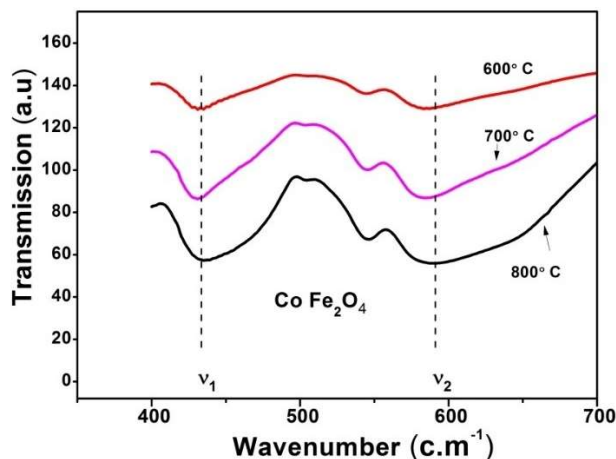


Fig. 5. FTIR spectrum of CoFe_2O_4

The FTIR absorption spectra for CoFe_2O_4 (for 600-800°C) are shown in Fig. 5, for frequency range (400 - 700 cm^{-1}). For Cobalt ferrite, two important infrared peaks are obtained at wavenumber 439 cm^{-1} (ν_1) and 602 cm^{-1} (ν_2) for bonds present at the octal and tetrahedral places respectively. The wavenumber 602 cm^{-1} is utilized in calculating the tetrahedral bond length of (Fe-O), and (Co-O) [18]. Tetrahedral site has got greater vibrational frequency than the octal site, as bond length of the octal sites is larger comparatively.

We can observe in Fig. 5, the absorption peaks gradually shift towards a lower wavenumber value with the increase in calcination temperature. The stretching of the metal-oxygen bond, due to propagated crystal strain in materials with annealing, may be a probable reason for this shift.

3.4 Magnetic Properties

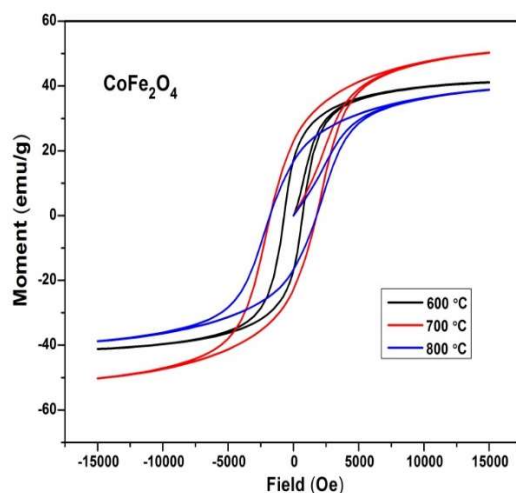


Fig. 6. MH loops at room temperature for CoFe_2O_4 (for 600-800°C)

Fig. 6 shows the magnetic hysteresis (MH) loops of CoFe_2O_4 samples. The ferrimagnetic behavior and moderate coercivity values are shown by hysteresis curves. Hysteresis curves frequently become saturated in the ± 1.5 Tesla applied magnetic field. With an increase in calcination temperature, remanent magnetization (M_r) decreased and magnetization (M_s) increased. We are aware that Fe^{3+} dipole moments are parallel to the c axis and that super exchange motions with O^{2-} ions amplify them [19-20]. It's noteworthy that coercivity values rose monotonically with calcination temperature. The increased magnetoanisotropy in nanomaterials with thermal activations is a major contributing factor to the higher coercive field [21]. The increasing magnetic moment is what causes the magnetization to be worth more, as we are aware that the magnetization effect and the magnetic moment have a linear connection [22].

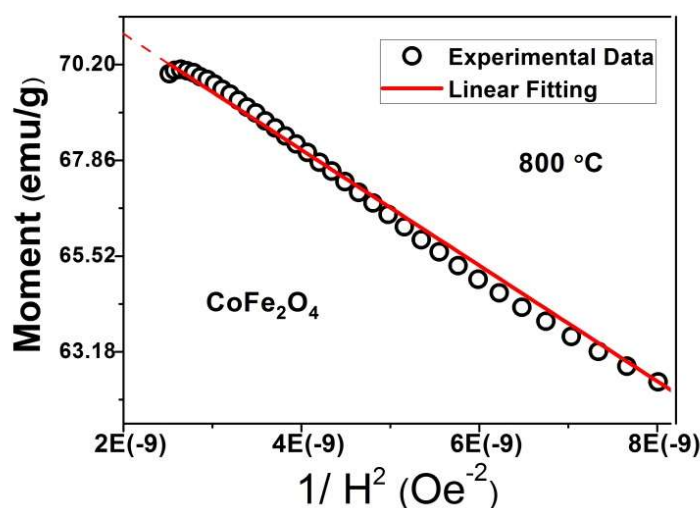


Fig.7. Moment vs H^2 for CoFe_2O_4 calcined at 800°C

The anisotropy is expressed as equation [18]

$$B = H_a^2/15 \quad (4)$$

The magneto anisotropy is calculated using expression

$$H_a = (2K_1)/M_s \quad (5)$$

The intercept on the y axis of the linearly fitted curve of the Magnetization versus $(1/H^2)$ plot (Fig. 7) determines the value of magnetization (M_s). The magneto anisotropy field (B_1) is given by the slope of linearly fitted curve. Further using equations (4) and (5) we get magnetocrystalline anisotropy (K_1). All the magnetic parameters are enlisted in Table 2.

Table 2. Magnetic parameters details of CoFe_2O_4

Calcination($^\circ\text{C}$)	Magnetization (M_s)(emu/g)	Retentivity (M_r)(emu/g)	Squareness ratio	Coercivity H_c (Oe)	Anisotropic constant
---------------------------------	-----------------------------------	---------------------------------	---------------------	--------------------------	-------------------------

					K_I $\times(10^6$ $\text{erg/cm}^3)$
600	47.62	21.19	0.44	454	4.61
700	69.34	36.01	0.51	1438	8.11
800	71.11	37.16	0.52	1467	8.77

The observed rise in M_s , which ranges from 47.62 to 71.11 emu/g, may be caused by increased lattice strain. Since these nanomaterials have a greater coercivity value of order 1467 Gauss, it is possible that they could be useful in applications requiring perpendicular recording media [23-24]. This implies that CoFe_2O_4 would be chosen for use as a permanent magnet and magnetic field generator.

Conclusions

Utilizing the citrate precursor sol-gel technique, CoFe_2O_4 was created. Spinel crystal symmetry that is indexed to the $Fd3m$ space group is present in all samples. The calcination process caused an increase in the lattice volume and edge parameters (a). With rising temperature, the Cobalt lattice's crystallite size and lattice strain also significantly rise in produced nanomaterials. The FTIR spectrum and the XRD data are in agreement. The highest saturation magnetization levels, in the range of 71.11 emu/g, are found in cobalt ferrites calcined at 800°C. Cobalt ferrites (800°C) also have the greatest values for coercivity of magnitude 1467 Gauss. It has been noted that cobalt ferrite calcined at 800°C has the highest magnetism and anisotropy values but is comparable for sample 700°C. One cause, suggested by a rise in the exchange contacts between iron ions, may be the increase in the Fe^{3+} ions. The current work provides a window into how lattice strain brought on by calcination can improve the structural and magnetic characteristics of nanocrystalline cobalt ferrite.

Acknowledgments

Authors are thankful to IIT BHU for providing lab facilities.

References:

1. Akhlaq Hussain, Abdul Naeem, Journal of Materials Science: Materials in Electronics (2018) 29:20783–20789, <https://doi.org/10.1007/s10854-018-0220-9>
2. V. Pillai, D.O. Shah, J. Magn. Magn. Mater. 163(1996)243–248, [https://doi.org/10.1016/S0304-8853\(96\)00280-6](https://doi.org/10.1016/S0304-8853(96)00280-6)
3. J. Ding, T. Reynolds, W.F. Miao, P.G. McCormick, R. Street, J. Appl. Phys. Lett. 65, 3135–3136 (1994), <https://doi.org/10.1063/1.112459>
4. K. Raj, B. Moskowitz, R. Casciari, Advances in ferrofluid technology, J. Magn. Magn. Mater. 149(1995)174–180, [https://doi.org/10.1016/0304-8853\(95\)00365-7](https://doi.org/10.1016/0304-8853(95)00365-7)
5. C.Dey, K. Baishya, A. Ghosh, M.M Goswami, A. Ghosh. K., Mandal, J. Mag. Mag. Mater. 427, 168-174 (2017), <https://doi.org/10.1016/j.jmmm.2016.11.024>

6. Fadi Choueikani, François Royer, Damien Jamon, *Appl. Phys. Lett.* 94, 051113 (2009), <https://doi.org/10.1063/1.3079094>
7. S. G. Kakade, Y. R. Ma, R. S. Devan, *J. Phys. Chem.C* 120, 5682 (2016).<https://doi.org/10.1021/acs.jpcc.5b11188>
8. S.Supriya, Sunil kumar, M.kar, *J.of Mater. Science, Mater. in Electronics* 28, pages10652–10673(2017), DOI: 10.1007/s10854-017-6841-6
9. F. Bentivegna, M. Nyvlt, *J.of Applied Physics*, 85(1999)2270, <https://doi.org/10.1063/1.369537>
10. I.C.Nlebedimn , N. Ranvah, P.I. Williams, *Journal of Magnetism and Magnetic Materials* 322 (2010) 1929–1933, <https://doi.org/10.1016/j.jmmm.2010.01.009>
11. Lawrence kumar, M. Kar, *IEEE Transactions on Magnetics*, Vol 47(2011)**3645**–3648, <https://doi.org/10.1109/TMAG.2011.2151841>
12. Rajnish Kumar, Manoranjan kar, *Ceramics. International*, 42(2016)6640-6647,<https://doi.org/10.1016/j.ceramint.2016.01.007>
13. Rajnish kumar, R.K.Singh, Mukesh K. Zope, Manoranjan Kar, *Mater. Science and Engg. B*, 220, (2017)73-81, <https://doi.org/10.1016/j.mseb.2017.03.012>
14. Rajnish kumar, M.Kar, Lattice strain induced magnetism in substituted nanocrystalline cobalt ferrite, *J. of Mag. and Mag. Mater.*,vol 416, (2016)335-341, <https://doi.org/10.1016/j.jmmm.2016.05.035>
15. M.H. Sousa, F.A. Tourinho, *J. Phys. Chem. B*, 105 (2001), 1168–1175.
16. Y.Liu, Y. Zhang, J.D. Feng, *J. of Exper. Nanoscience* Vol. 4, No. 2, June 2009, 159–168, <https://doi.org/10.1080/17458080902929895>
17. I.C.Nlebedim, D.C. Jiles, *J. Appl. Phys.*, vol. 117, 17A506 (2015). Thermal effects on the magnetic properties of titanium modified cobalt ferrite, <https://doi.org/10.1063/1.4919229>
18. H. Y. He, *J.Mater. Manufacturing Processes*, Vol 27(9), 2012, 901–904. doi:10.1080/10426914.2011.610086
19. S.Ounnunkad,P.Winotai, *Journal of Magnetism and Magnetic Materials*.301(2006)292-300. <https://doi.org/10.1016/j.jmmm.2005.07.003>
20. H.J.Kown, J.Y.Shin, J.H.Oh, *J.Appl.Phys.* 75(1994)6109. <https://doi.org/10.1063/1.355476>
21. D.M.Hemeda, A.Al-Sharif, O.M.Hemeda, *Journal of Magnetism and MagneticMaterials*, 315, L1-L7 (2007). <https://doi.org/10.1016/j.jmmm.2006.12.019>
22. A.M.Alsmedi,I.Bsoul,S.H.Mahmood,G.Alnawashi,K.Prokes,K.Siemensmeyer,B.Klemke , H.Nakotte, *J.Appl.Phys.*114 (2013)243910.
23. Heiba, Z. K., Mostafa, N. Y., and Abd-Elkader, O. H., *J. Magn. Magn. Mater*, vol. 368(2014), pp. 246–251. <https://doi.org/10.1016/j.jmmm.2014.05.036>
24. Zaki, H. M., Al-Heniti, S. H., and Hashhash, A., *J. Magn. Magn. Mater*, vol. 401(2015), pp. 1027– 1032. <https://doi.org/10.1016/j.jmmm.2015.11.021>